LHCb Collaboration

LHCb 2001-039 VELO
4th May 2001

Performance of an irradiated n–on–n Hamamatsu prototype VELO detector

T. Bowcock [1] J. Buytaert [2] G. Casse [1] M. Charles [3] H. Dijkstra [2] P. Collins [2] O. Dormond [4] M. Ferro-Luzzi [2] F. Fiedler [2] R. Frei [4] G. Gagliardi [4] P. Jalocha [5] J. Libby [2] T. Ketel [6] C. Parkes [1] U. Parzefall [1] T. Ruf [2] M. Tareb [4] F. Teubert [2] V. Wright [1] M. Witek [5]

Abstract

An n–on–n design LHCb PR-01 prototype VELO detector was irradiated and equipped with LHC speed electronics. This detector was successfully operated in a test-beam and its performance assessed.

After an irradiation dose corresponding to approximately two years of LHCb operation ($3 - 4 \times 10^{14}$ protons/cm^2) full charge collection was obtained at 220 V and no degradation in resolution was observed. A signal-to-noise ratio, at full charge collection efficiency, of 21.5 was achieved. This impressive performance strongly supports the use of detectors of a similar design for LHCb.

[1]University of Liverpool, Oliver Lodge Laboratory, Liverpool, England
[2]CERN, CH-1211, Geneva 23, Switzerland
[3]Department of Nuclear and Particle Physics, Oxford University, 1 Keble Road, Oxford OX1 3RH, England
[4]Institut de Physique des Hautes Energies, Batiment des Sciences Physiques, Université de Lausanne, CH-1015 Dorigny 20, Switzerland
[5]Institute of Nuclear Physics High Energy Departments, ul. Kawiory 26 A, 30-055 Kraków, Poland
[6]NIKHEF, Kruislaan 409, 1098 SJ Amsterdam, The Netherlands

1 Introduction

In August 2000 an irradiated Hamamatsu LHCb VELO PR-01 prototype detector was operated in a test-beam of 120 GeV muons and pions at the CERN SPS. The primary goals of the test-beam were to measure the efficiency and resolution of the detector after irradiation conditions corresponding to more than one year[1] of operation in LHCb.

2 Detector Description

2.1 Detector Design

The tested detector was h-14-ϕ. This is a 1998 PR-01 prototype ϕ type detector [1, 2] manufactured by Hamamatsu Photonics[2]. The geometrical properties of the radial (R) and azimuthal (ϕ) measuring sensor designs are illustrated in Figure 1, further details are available in [3]. The detector contained separate strips in inner and outer regions. The strips ran approximately radially on the detector and hence the inter-strip pitch varied uniformly along the length of the strip, with minimum values of 45 μm at a radius of 10 mm and 44 μm at 28 mm. The maximum radius was 5 cm and the angle covered by the detector was 72°. The 1024 read-out pads were arranged on a line outside the outer radius of the detector. The pitch of the read-out pads was 50 μm (in two staggered rows of 100 μm). The strips from the inner region were connected to the read-out pads using routing lines arranged on a second metal layer of the detector.

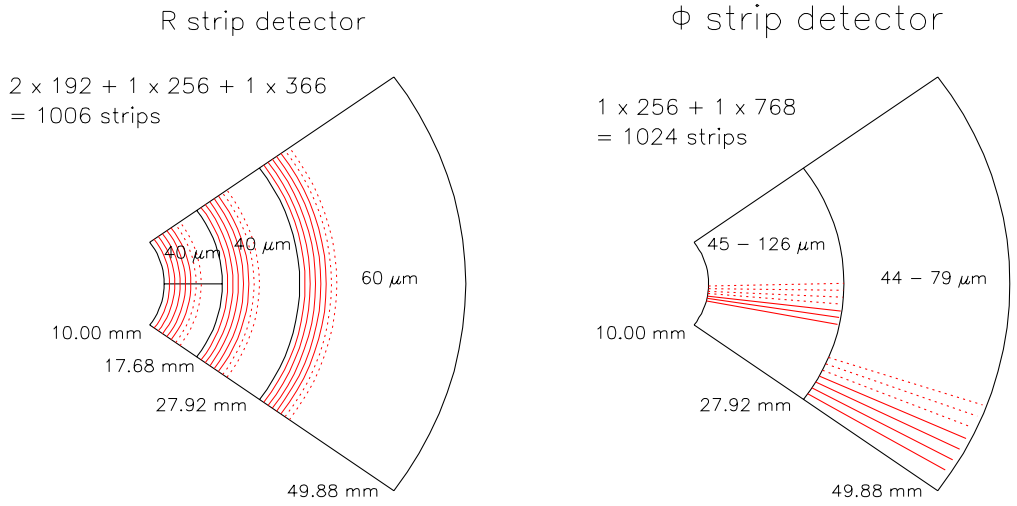

Figure 1: Strip layout of Hamamatsu prototype detectors. Detectors of both designs were used in the telescope stations. The irradiated test detector was of the ϕ design.

The detector was an n–on–n design, with individual p-stops and a thickness of 300 μm. These silicon detectors did not have an enhanced oxygen level.

[1] A peak fluence, at the inner radius of the detector, of less than 2×10^{14} protons/cm^2 per year is anticipated.

[2] 325-6,Sunayama-cho, Hamamatsu City, Shizoka Pref., 430-8587, Japan

2.2 Electronics

The sensor was read out using the SCT128A chip [5] and specially manufactured hybrids based on an ATLAS design. The hybrids were not perfectly matched to the detector, with an input pitch of 80 μm and only 3 chips per hybrid (384 channels). However, it was still possible to read out a section of the detector scanning irradiation intensities from 0 to 4×10^{14} protons/cm^2. The SCT128A was operated with an LHC speed (40 MHz) clocking rate.

3 Irradiation and Annealing

3.1 Irradiation

The detector was irradiated in a 24 GeV proton beam at the CERN PS irradiation facility in July 2000. The irradiation procedure and measurement of the beam profile is described in [4]. The detector received a peak fluence of $4.1 \pm 0.4 \times 10^{14}$ protons/cm^2. A Gaussian beam profile with a 6.1 ± 0.3 mm width was measured. A map of the irradiation profile of the detector was produced and is shown in Figure 2.

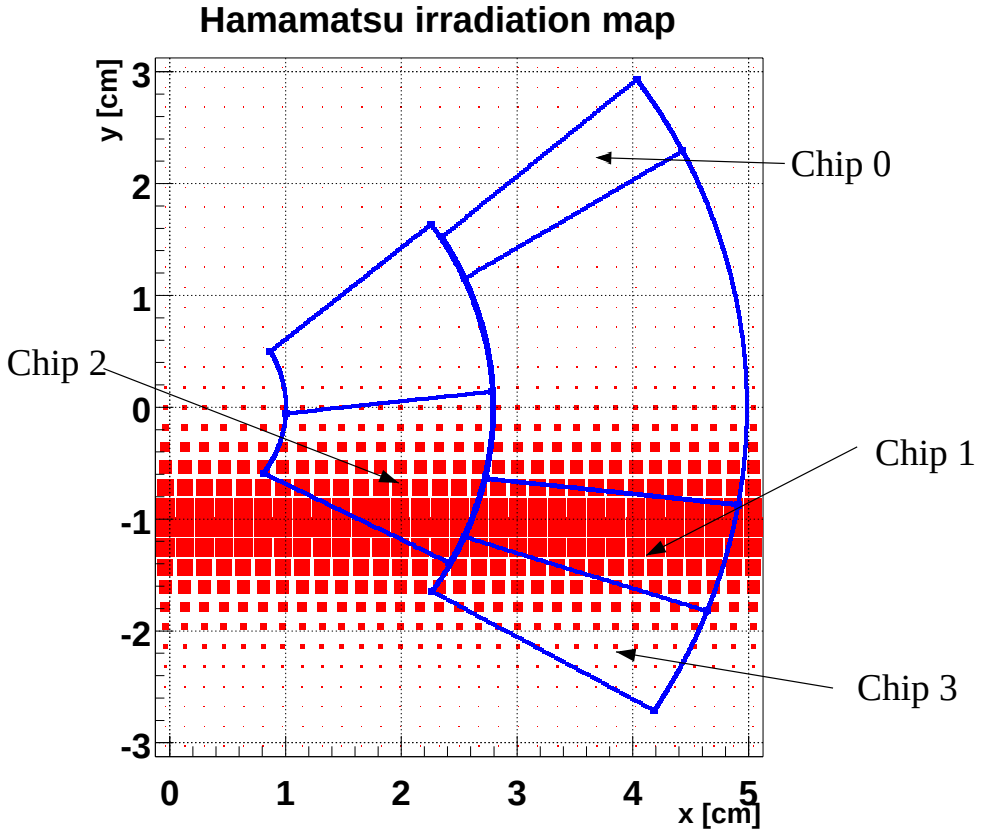

Figure 2: Positions of the instrumented regions of the test detector, with the irradiation dose received in different parts of the detector superimposed. The area of the shaded squares is proportional to the irradiation dose received at that point.

3.2 Annealing

The temperature of the detector was monitored during the irradiation procedure and prior to the collection of data in the test-beam. The temperature of the detector during all periods where it was above 0^0C is shown in Figure 3(a). The detector was usually kept below -10^0C.

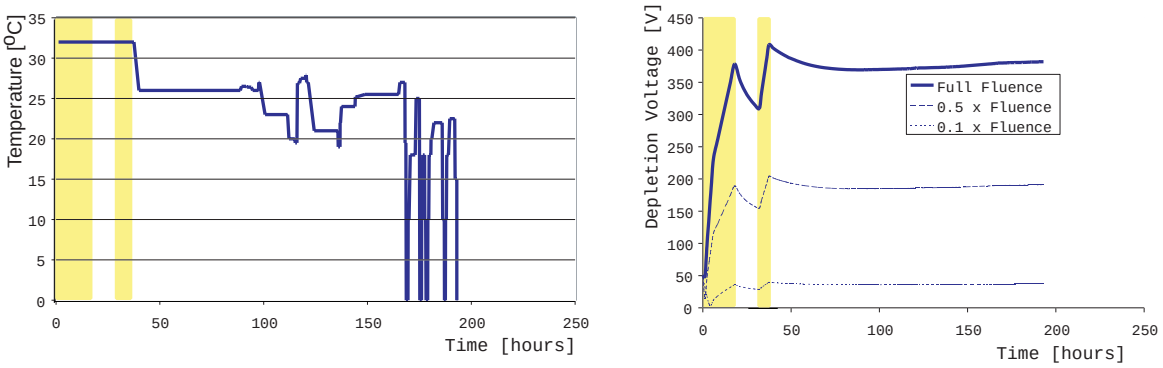

(a) (b)

Figure 3: The period that the detector spent above 0^0C during and after irradiation is shown in (a). The expected depletion voltage of the sensor is shown during the same period for a range of fluences in (b). The shaded area indicates the time when the detector was being irradiated.

A phenomenological parametrisation of the bulk radiation damage to silicon has been developed by the Hamburg group of the ROSE Collaboration [6]. The model is based on experimental results from the study of silicon diodes. Using this model, the evolution of the depletion voltage of the device has been simulated and is shown in Figure 3 (b) for a range of fluences. The model parameter values were taken from [7]. Final depletion voltages of 382 V, 191 V and 37 V are expected for the peak irradiation dose, 50% fluence and 10% fluence. The irradiation of the detector was interrupted after 18 hours and no beam was then available for a 14 hour period - the resulting kink in depletion voltage is clearly visible in Figure 3 (b).

The final depletion voltage of the device, after type inversion, is predicted to be insensitive to the initial depletion voltage. The impact of measurement errors on the temperature and time profile and the time the detector spent refrigerated were found to be negligible. However, the 8% uncertainty on the irradiation fluence corresponds to a similar uncertainty on the depletion voltage. The model predicts a very significantly improved performance for oxygenated silicon over standard silicon under proton irradiation: under the same conditions the expected final depletion voltage of an oxygenated detector would be 110 V. The model parameters have a significant variation between materials, changing individual parameters by the ranges reported in [7] and its references commonly result in changes of ± 50 V in the depletion voltage and an uncertainty of 100 V is not excluded. Furthermore, the model does not differentiate between n–on–n and p–on–n detectors, however significantly improved performance of irradiated n–on–n over p–on–n detectors has been reported [8]. In all the scenarios considered the final depletion voltage was found to lie in a fairly stable area on the reverse annealing slope just above the local minima of

the curve.

4 Test-Beam Setup

4.1 Beam Telescope

The test-beam infrastructure is illustrated in Figure 4.

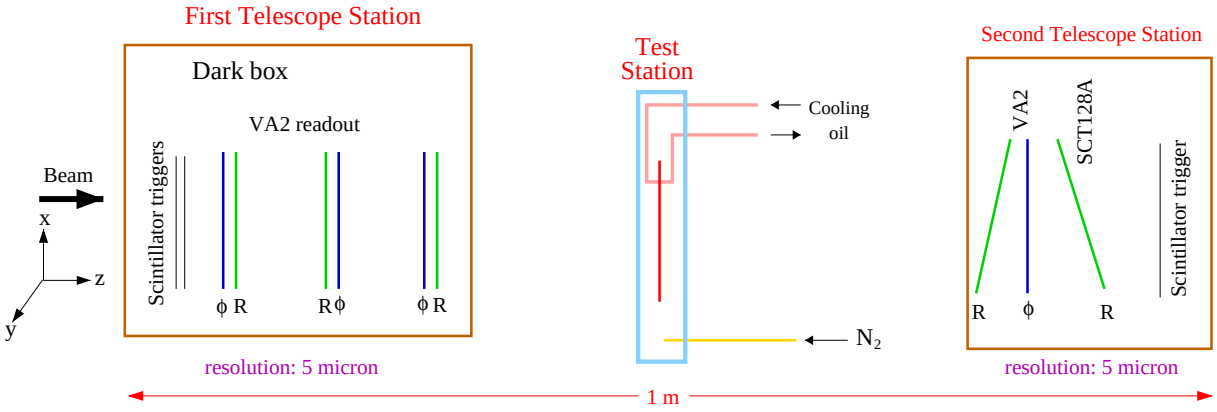

Figure 4: Arrangement of the detectors in the test-beam.

The light-tight box labelled in the diagram as "First Telescope Station" contained three pairs of R and ϕ non-irradiated Hamamatsu prototypes of the design shown in Figure 1. In addition, the box contained a pair of scintillators specially shaped to cover the detector regions with radius greater than and less than 30 mm. Thus tracks can be selected which pass either through the whole telescope acceptance, or just the more precise 40 μm pitch region on the inner part of the R detectors. These telescope stations have been used in previous test-beams and their performance is described in [9].

The box labelled "Second Telescope Station" was placed on the opposite side of the test detector. It contained another pair of R and ϕ detectors which were placed at specific angles to the beam-axis. This inclination optimises the detector resolution and, with just one detector for each coordinate, matches the precision of the first telescope station. The angles were chosen to optimise the resolution for the mean detector pitch, following the study described in [10], and were about 0.1 rad about the y axis for the R measuring detector and 0.2 rad about the x axis for the ϕ measuring detector. A second large scintillator was located in front of the second telescope station.

The fiducial area defined by the telescope was about 5 cm^2 for the more precisely measured inner region, which in practice was reduced due to the imperfect overlap achieved between the first and second telescope stations. The telescope design aimed to achieve a track extrapolation error at the test detector of around 4 μm for the most precisely measured tracks.

The telescope detectors described above were equipped with slow VA2 electronics. However, the second telescope station also contained an extra R measuring detector equipped with SCT128A electronics. This detector was read out to a six-chip hybrid using a custom designed fan-out. This fan-out facilitated the reading out of the whole

of the more precise inner region of the detector. This extra detector served as a reference for the timing of the SCT128A read-out of the test detector. Furthermore, in a multi-track event this detector allowed the unambiguous selection of which telescope track corresponded to the trigger of the SCT128A read-out; this is discussed further in Section 6.

4.2 Test Station

The irradiated test detector was located in an insulating box, labelled "Test Station" in Figure 4. The detector was mounted on an aluminium plate cooled with circulating oil from a fridge, and kept in an atmosphere of cool dry nitrogen. Temperature probes were installed on the detector, the cooling plate, and on the inside and outside of the box. The operating temperature of the detector was about -12° C. The set-up is shown in the photograph in Figure 5.

Figure 5: The irradiated test detector in its insulating box. The box containing the second telescope station is visible behind the insulating box. The fridge is visible in the top right of the photograph along with the pipes connecting this to the test detector.

The detector was equipped with SCT128A 3-chip hybrids. The regions of the detector which were read out are illustrated in Figure 2. During the first part of the test-beam the

detector was bonded to three chips. These chips read out the areas 1, 2 and 3 indicated in Figure 2. Unfortunately, chip 1 was non-functional throughout the test-beam. In the second part of the test-beam an area on the non-irradiated side of the detector was read out: this area is labelled Chip 0 in Figure 2.

Having performed the alignment (see Section 5), the position of the detector relative to the tracks observed in the telescope is illustrated in Figure 6. This figure is produced with the data collected during the first period of the test-beam. The area covered corresponds to chips 1 and 3. As chip 1 was non-functional, the only useful data for the charge collection efficiency analysis (see Section 7) were those taken with chip 3. However, data from chip 2 was used for studying noise values, as discussed in Section 10. In a later part of the test-beam tracks were also obtained covering the non-irradiated Chip 0 region.

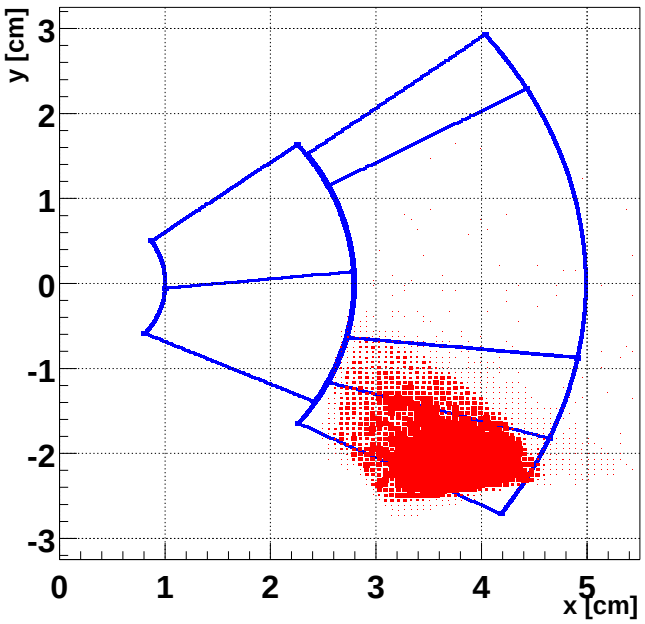

Figure 6: Overlap of reconstructed telescope tracks with the irradiated test detector

4.3 Trigger

The SCT128A electronics used in the test detector were clocked at the full LHC speed of 40 MHz. The front-end amplifier rise-time of the VA2 system, used for the telescope, was 1 μs.

A scintillator trigger signal was generated if co-incident pulses were obtained from the scintillators located at the near and far side of the telescope detectors. The scintillator pulses were of a few ns duration. The co-incidence was achieved by delaying the scintillators pulses to account for their spatial separation and non-equal cable delays.

The triggering system required a signal from the scintillator co-incident with the SCT128A trigger accept time window. This window was opened every 200 ns, for a duration of typically 75 ns which was tunable in 25 ns steps. The time between opening the trigger window and the SCT128A read-out was adjustable in 1 ns steps. By tuning

this parameter the trigger acceptance window was centred on the peak of the SCT128A pulse, and due to the extent of the time window the full SCT128A pulse shape could be observed. Thus, the read-out cycle occurred at a 5 MHz rate, and this was in phase with the SCT128A clock. Hence only one eighth of the 128 SCT128A pipe-line locations were used.

Once a trigger had been accepted the analogue signals from all channels of all detectors were read out, digitised, and stored to disk for later analysis. This read-out cycle introduced a busy period and no further triggers were accepted until after this was complete. The maximum instantaneous data taking rate achieved was 55 Hz, with an overall rate (taking into account the SPS spill separation) of 8Hz (30,000 events/hour).

5 Alignment

The raw data of the detectors was processed with pedestal subtraction and common mode noise suppression algorithms. Hit strips were then identified on the detectors and adjacent hits joined to form clusters. Tracks were then fitted through the clusters on the eight telescope detectors [11]. The reliable relative alignment of the telescope detector has been reported previously [9].

The irradiated detector was then aligned to these tracks. The tracks were extrapolated to the test detector and a nearby cluster on this detector identified. The residual between the cluster and track extrapolation point is computed and divided by the estimated error on the cluster position. A χ^2 is formed by summing these quantities for a set of selected tracks. The six degrees of freedom describing the location of the test detector are treated as free parameters and the χ^2 minimised.

The resulting alignment is of poor quality, but sufficient for the charge collection efficiency (CCE) and cluster shape analysis described in this paper: it is illustrated in Figure 7. The non-irradiated timing station was aligned by the same procedure.

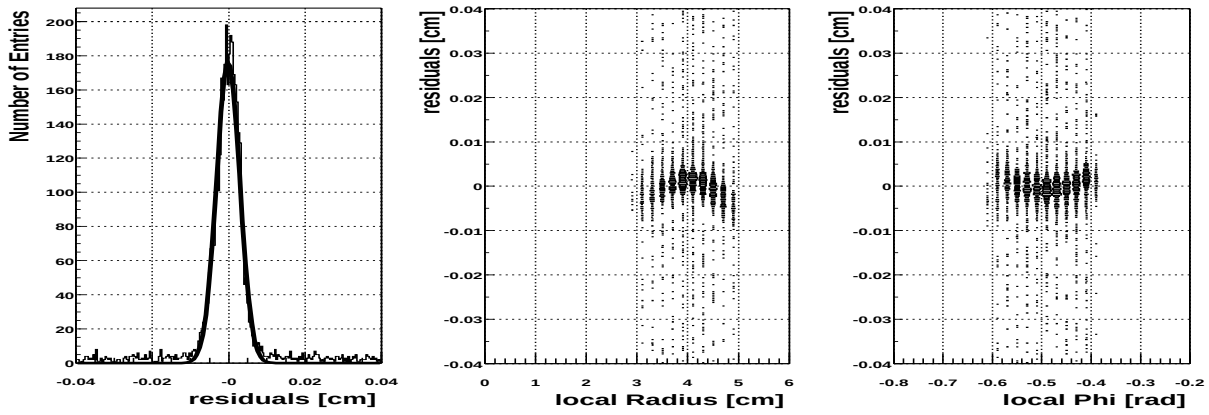

Figure 7: Alignment quality of the irradiated Hamamatsu detector. The overall residual is 28 μm and there are variations of up to 50 μm as a function of R and ϕ.

6 Track Selection

The charge collected on the test detector by a traversing track was calculated by extrapolating the telescope track to the aligned test detector and summing the charge on the strips adjacent to the intercept point, as discussed in Section 7. In order to be able to measure very low charges a cleaning procedure must be applied to the data sample, otherwise the results may be distorted by bad data or geometrical edge effects. Hence, the aim of the cleaning was to ensure that the only reason to measure low charge is due to true detector inefficiencies. Bad runs were removed (2 out of 27 runs) and a search was performed for dead strips on the test detector, but none were found.

The following fiducial cuts were applied to the track extrapolation point in the local detector frame:

- $2.8 < R < 4.8$ cm
- -0.6 rad $< \Phi < -0.36$ rad.

After these cuts the signal reconstructed in the irradiated detector is illustrated in Figure 8 (a).

The full extent of the trigger time window (as discussed in 4.3), labelled as TDC time, is observed in this figure. However, for the CCE studies it is best to select the peak of this distribution. A cut was made that the track should arrive within the following time window:

- $0 <$ TDC time < 20 ns.

This cut is sufficient for studies of the CCE and cluster shape as a function of voltage and irradiation. In order to determine the optimum signal-to-noise of the detector, a more narrow window was used, as described in Section 10.

A band of entries at zero charge is clearly visible in Figure 8 (a). This is largely due to reconstructed telescope tracks which are out-of-time with the SCT128A. Despite the timing cuts these telescope tracks may still occur as multiple tracks may be reconstructed in a single event. The long (~ 1 μs) integration time of the VA2 electronics telescope leads to the reconstruction of these tracks that are out-of-time with the scintillator trigger and the SCT128A read-out as well as the true track that caused the read-out trigger. If the out-of-time track is within the fiducial area of interest it will also appear in Figure 8. The number of reconstructed tracks and clusters is shown in Figure 9 for a typical test-beam run using an incident pion beam. The clusters reconstructed in the telescope of 8 detectors shows peaks at 8 and 16 clusters[3] and the fraction of events with 2 tracks is typically 20%; for some runs this fraction increased to as high as 50%.

The SCT128A equipped non-irradiated timing station was used to select the true in-time track. The effects of applying cuts to this station are shown in Figure 10. In part (a) the charge seen in the irradiated detector for tracks within the fiducial time and space cuts is shown. The effect of applying the additional cut that the charge measured in the fast station is over 30 ADC counts is shown in part (b). The peak at zero is reduced from 24% of entries to 4% by this cut. The remaining proportion of the peak at zero is

[3]More than two tracks may however be reconstructed in the event due to split clusters in the telescope. This problem is under investigation.

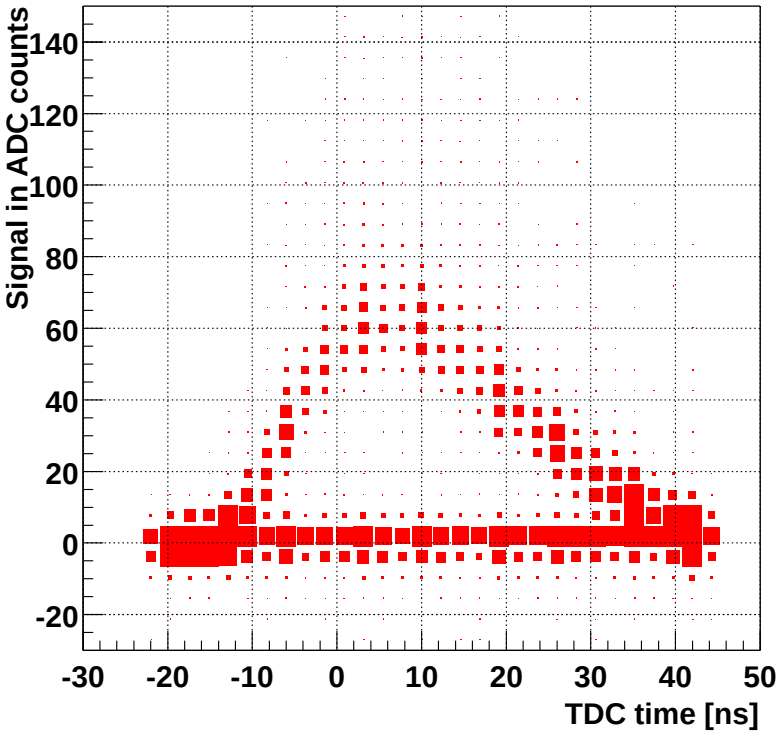

(a)

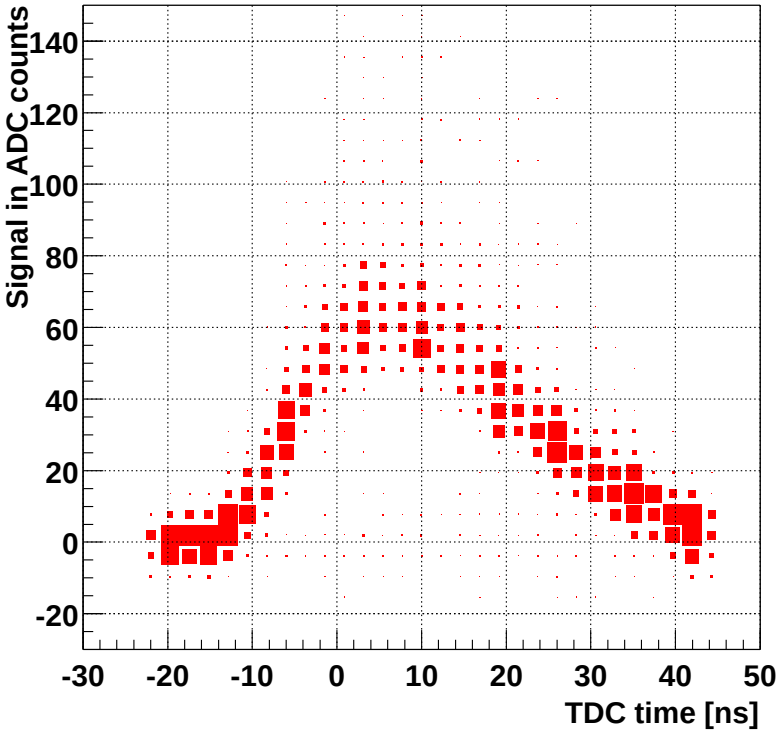

(b)

Figure 8: Signal reconstructed in the irradiated test detector as a function of time. In (a) the distribution is shown after applying only fiducial cuts, the line at zero charge is due to out-of-time tracks (see text). In (b) the applied set of cuts correspond to (d) from Figure 10 without the cut on the TDC time. Note that only the relative timing is shown: the zero point has no special significance.

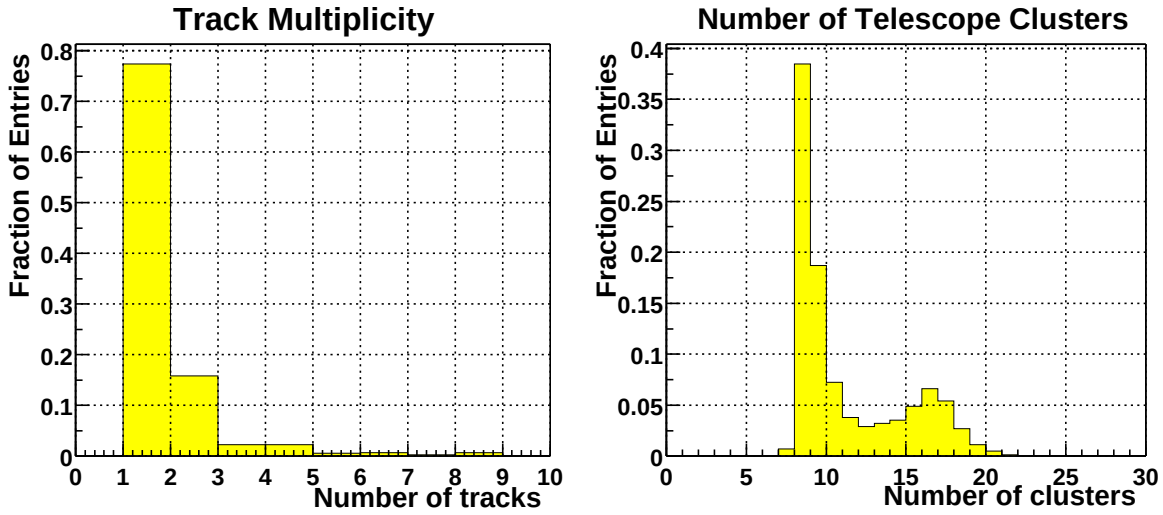

Figure 9: Typical distribution of reconstructed tracks (a), and reconstructed clusters (b) in the telescope of eight detectors, for a test-beam run with an incident pion beam

attributed to tracks which are not in good time but still, due to the long Landau tail, give a high charge in the timing station. The peak can be further reduced by selecting only the track which deposits the highest charge in the timing station; the peak at zero drops to 1% of the tracks (illustrated in part (c)). A reduction to 0.1% can be achieved by selecting only events which have exactly one track, and less than 11 clusters in the telescope, this is illustrated in Figure 10 (d). However, in order to keep high statistics, the set of cuts corresponding to part (c) of Figure 10 were used for the analysis reported below.

Note that for studies of the SCT128A pulse shape [12] it is not possible to cut on the signal in the fast station; for these studies the cuts corresponding to part (d) of Figure 10 were applied. The resulting time distribution of the signal in the irradiated detector is shown in Figure 8 (b).

After the set (c) cuts were applied a total of 10,516 tracks were reconstructed traversing the irradiated detector, out of a total of 250,000 triggered events on tape.

7 CCE Measurement

The charge collected on the irradiated detector was measured by summing the signal seen in strips around the intercept point of an extrapolated telescope track. With this method it is possible to measure the CCE even when the signal-to-noise ratio is very low. The CCE was measured both as a function of irradiation and of voltage. For this analysis the charge was summed from the five strips closest to the intercept point. This achieves sufficiently low noise (about 18000 electrons, or five ADC counts) and ensures that misalignment effects do not result in missed charge. In section 9 it will be shown that this method is appropriate even for the region of smallest inter-strip pitch and highest irradiation as all the charge is collected within five strips.

The function used to fit the charge distributions had a shape similar to a Landau

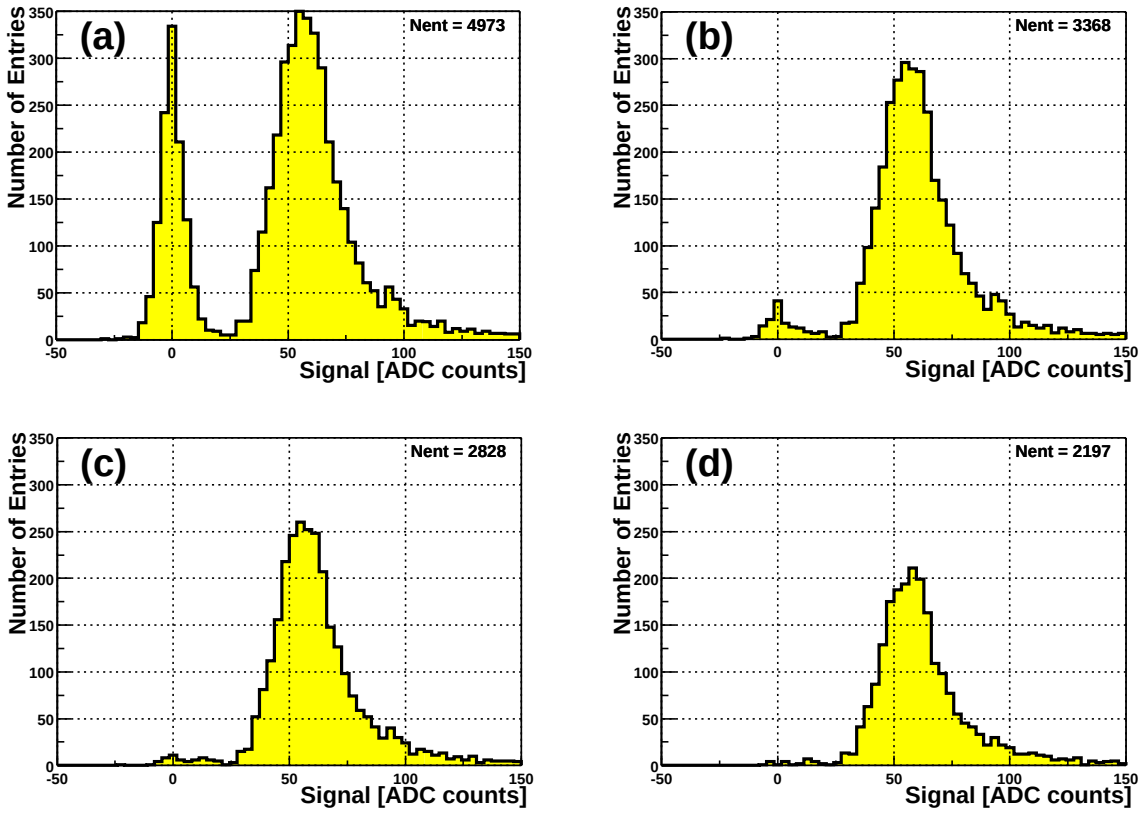

Figure 10: Charge reconstructed around telescope tracks intercepted at the irradiated detector, where the trigger is in-time, for (a) no additional cuts (b) requiring a large signal for that track in the fast station (c) selecting only the track which gives the largest signal in the fast station (d) selecting only events with exactly one track.

smeared with extra noise, it is defined as:

$$f(x) \propto e^{-(v(x)+e^{-v(x)})}$$

$$v(x) = (x - x_0)/w_{\pm}$$

where x is the charge in ADC counts, x_0 is the peak position and w is the width. Different positive width values are fitted (w_+ and w_-) in the regime $x > x_0$ and $x < x_0$. Note that v changes sign for x less than or more than x_0.

An example of the quality of these pseudo-Landau fits is illustrated in Figure 11, a good χ^2 per degree of freedom was obtained.

The data were divided into runs taken with different bias voltages on the irradiated detector and into regions of the detector that received different fluences. The most probable value of the Landau was obtained from fits to these data samples. The CCE values obtained are shown as a function of voltage for a range of irradiation doses in Figure 12. The voltage at which the full charge is collected, is estimated at about 50 V for the region of lowest irradiation, and 220 V for the region of highest irradiation. Unfortunately, it

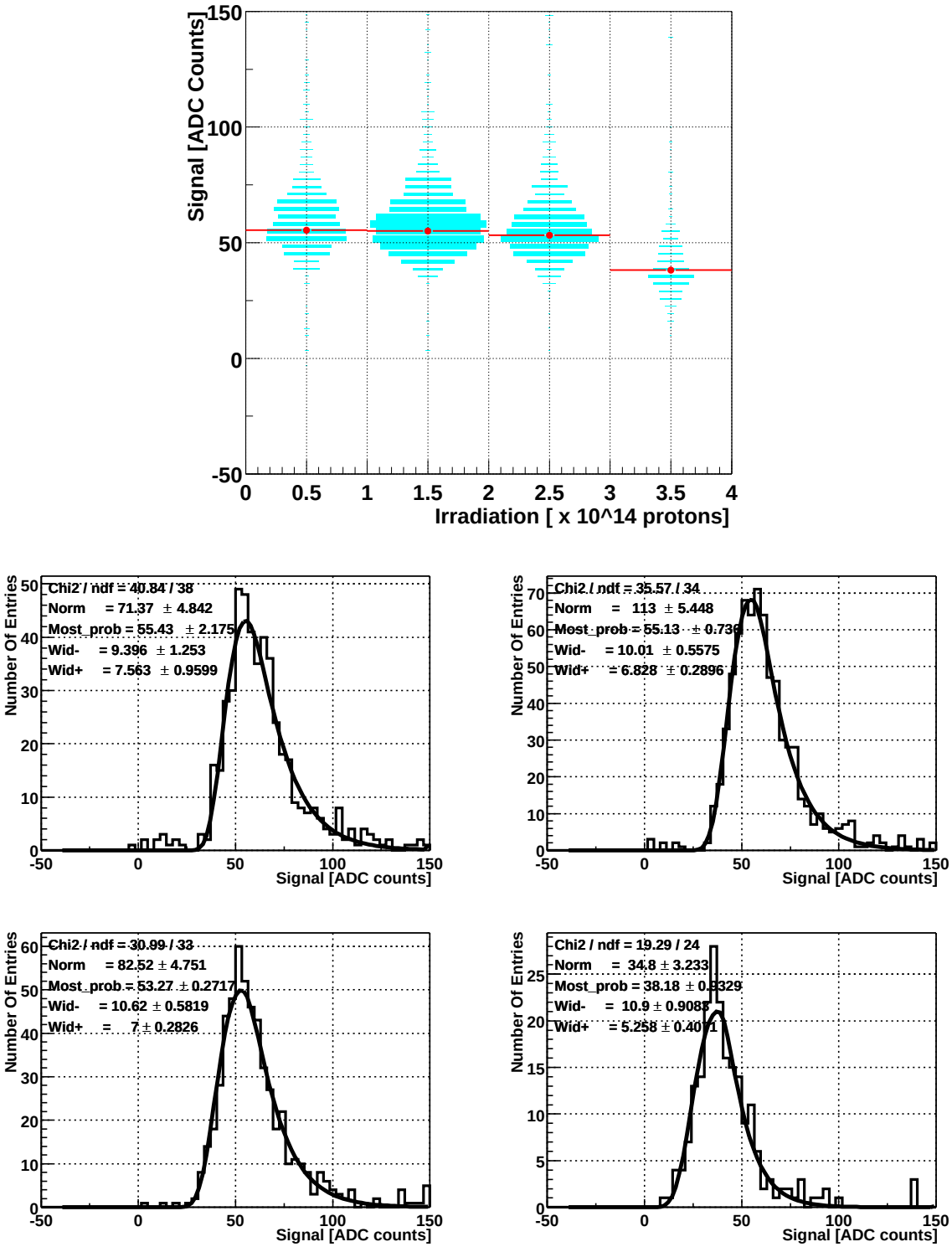

Figure 11: Example of a fit to the Landau distributions as a function of irradiation, for a voltage of 100 V. The top plot shows the original scatter plot and the result of fitting a Landau to each slice of irradiation dose. In the four lower histograms the fitted Landau in each irradiation slice is given.

was not possible to study the maximum CCE using the non-irradiated area of the test detector: this is discussed in section 10. However, the timing station gives an average of 58.5 ± 3 ADC counts from the peak of the Landau distribution, where the error includes the expected gain variation between chips. The timing detector is a non-irradiated detector of the same thickness and with identical SCT128A read-out and electronics chain to the test detector. This result confirms that all the charge was collected from the irradiated test detector.

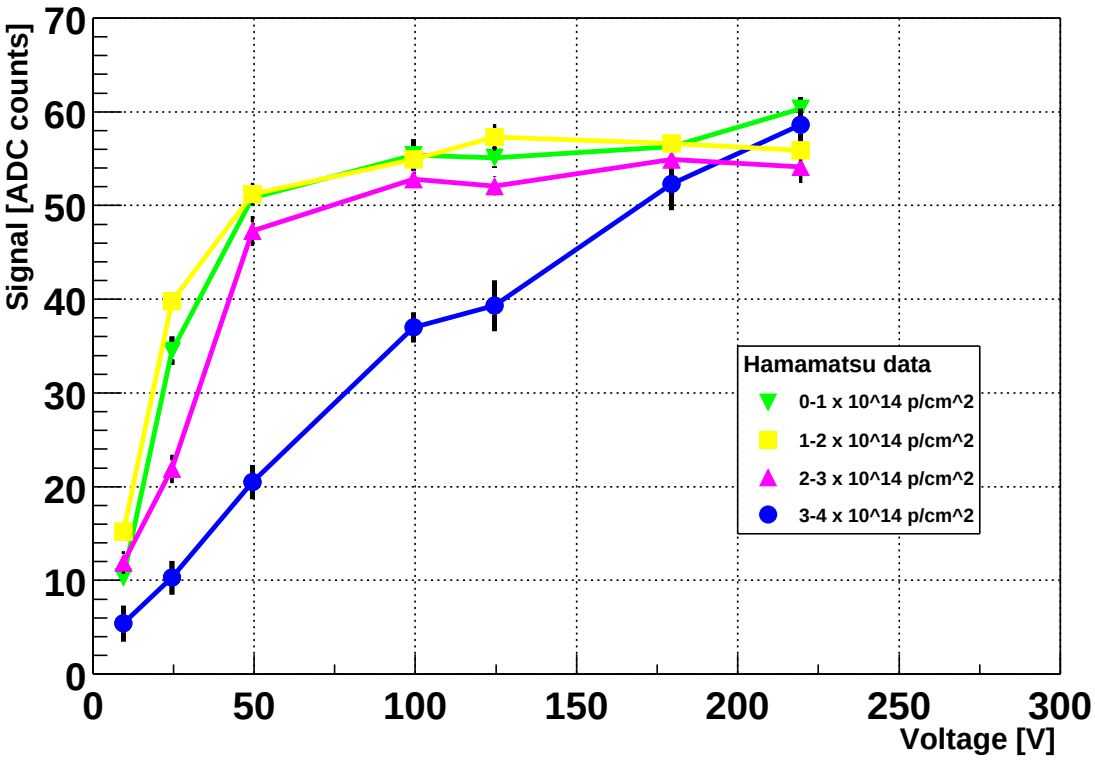

Figure 12: Signal reconstructed in the test detector, for different voltages and irradiation doses.

The depletion voltage of the device may be determined from the points measured in Figure 12. A straight-line fit was performed to the data points that lay below 90% of the maximum CCE point. The depletion voltage was taken from the intercept point of this line with the level of the maximum CCE observed, this is shown in Figure 13. Note, that due to charge trapping effects, it may be necessary to significantly over-deplete an irradiated detector before the full charge is collected. The significant errors on the depletion voltage reflect the range of values that would be obtained from alternative strategies, such as taking the voltage at which 80% of the charge is collected. In Figure 13 the data is compared with the depletion voltage model described in section 3.2 and may be seen to compare favourably. Recall that the model is based on tests of diodes, and that the depletion voltage was determined from the behaviour of the capacitance with voltage of these samples.

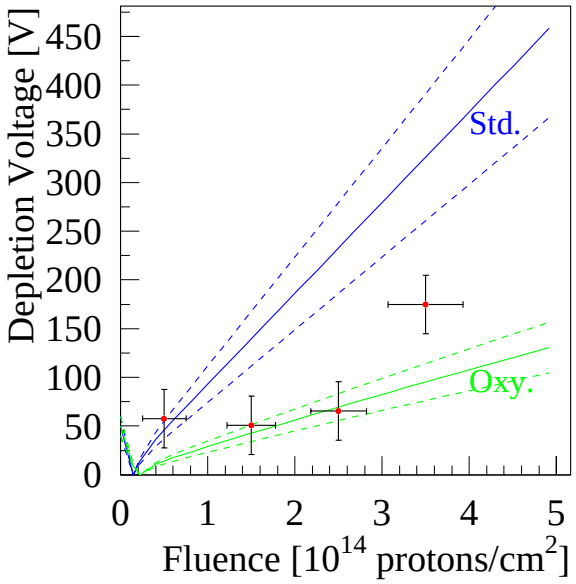

Figure 13: The depletion voltage with irradiation fluence is shown for the non-oxygenated test detector and compared with the expected performance for oxygenated and non-oxygenated diodes.

8 Efficiency Measurement

The most relevant quantity to LHCb operation is the efficiency with which a cluster can be reconstructed. First, pedestal subtraction and common mode noise suppression were applied to the ADC values obtained from each channel of the detector, the algorithm applied is described in [2]. Then, clusters were formed from the noise corrected hits. The central hit of a cluster was required to have a signal-to-noise greater than 1.5. Neighbouring channels for which the signal-to-noise exceeded 10% of that of the central strip were added to the cluster; up to two channels each side of the central hit were included in the cluster. A signal-to-noise cut may then be applied to the cluster.

Clusters on the test detector were accepted if they were reconstructed within 200μm of the extrapolated track. The probability of accepting a fake cluster when using a cluster signal-to-noise cut of 3 is approximately 20%. The results are shown in Figure 14, as a function of voltage and irradiation fluence, for different cuts on the signal-to-noise ratio of the cluster. It can be seen that even the most irradiated region reaches full efficiency for a signal-to-noise cut of 3 after only 50 V.

9 Cluster Shapes

As mentioned in Section 5 an optimal alignment of the system has not yet been achieved. The alignment problems lead to the dependence on R and ϕ of the track residuals shown in Figure 7. Hence, the intrinsic resolution of the detector is hidden by the error on extrapolating to and intercepting with the test detector. Due to these alignment problems it has not yet been possible to make a measurement of the dependence of the resolution

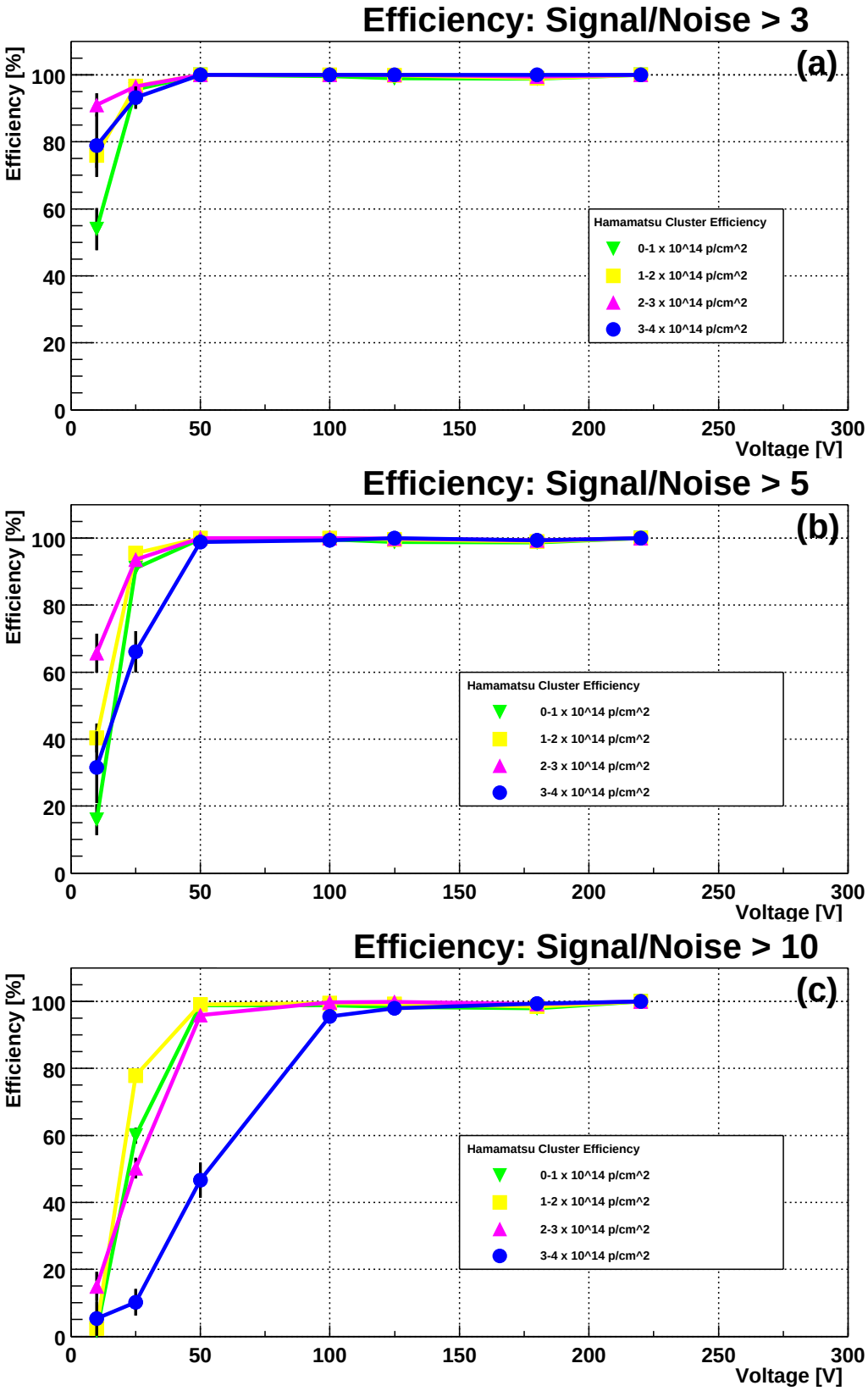

Figure 14: Cluster reconstruction efficiency as a function of bias voltage for a range of irradiation fluences. In plot (a) the signal-to-noise ratio of the cluster was over 3, for (b) this ratio was greater than 5 and in (c) exceeded 10.

on the irradiation and voltage. However, information can be obtained on the detector resolution by studying the cluster shapes.

The intrinsic resolution of the detector is related to the division of charge between strips: if the charge is spread over many strips the resolution is degraded. Thus, a study of cluster shapes was performed to investigate whether such spreading occurs for the test detector. The effects of bias voltage and irradiation fluence were considered. The variation in collected charge when summing the signals obtained from an increasing number of strips was analysed. If the full charge of a cluster is not collected when integrating over two strips this is evidence that the resolution is degraded by charge spreading. The details and results of this analysis are described below.

The selection of tracks is as described in Section 6 and used in the CCE analysis. The charge on 2, 4, 6, 8, 10 or 12 strips around the extrapolated track intercept point was summed. For the 2 strip case the intercepted strip and the nearer of the neighbouring strips to the intercept point were used. Then a strip on either side of these 2 was added for the 4 strip total and so on.

The data at an individual voltage point were divided into different levels of irradiation dose. For each irradiation level, the data sample at the finest pitch available with reasonable statistics was selected. As seen in Figure 2 the highest irradiated region ($\sim 4 \times 10^{14}$ protons/cm^2) of chip 3 is at smaller R than the less irradiated regions; hence, the finest pitch region is different for the different irradiations studied. Therefore, to allow comparison of the results, the cluster extent was defined as the number of strips summed over multiplied by the mean pitch for the region studied. The summed ADC distributions were then fitted with the same pseudo–Landau function as used in the CCE analysis.

Figure 15 (a)-(f) shows the most probable values of the pseudo–Landau fits against the cluster extent of the most ($> 3 \times 10^{14}$ protons/cm^2) and least ($< 1 \times 10^{14}$ protons/cm^2) irradiated regions. For clarity only the range 0 to $\sim 500\mu$m of cluster extent is shown. The graphs are shown for 6 voltage points: 25 V, 50 V, 100 V, 125 V, 180 V and 220 V. Over the whole range of voltages and irradiations the distributions are nearly flat. Hence, it is concluded that the intrinsic resolution for this prototype detector is not degraded by the sharing of charge between strips: this can be compared to the p–on–n prototype studied in [13].

10 Signal-to-Noise Performance

The SCT128A pulse shape from chip 3 of the test detector is shown in Figure 8 (b). A restricted time window was used to select data from the peak of the SCT128A pulse, the following results use data collected within a ± 1 ns period of the estimated maximum signal point. Fitting a pseudo–Landau distribution for the data collected at 220 V gives a most probable value of 58 ADC counts. The common mode suppressed noise measured on the strips was 2.7 counts. Hence, the signal-to-noise ratio for the over depleted detector was measured to be 21.5. This performance can be compared with that reported for a PR-02 p–on-n detector in [**?**]. The PR-01 n-on-n detector is seen to be significantly more noisy that the p–on-n design, although due to the 30

The chip-to-chip gain variation has been studied in laboratory tests and using the data on 5 chips of the timing station. This latter study is reported in [12]. A variation of less than $\pm 5\%$ was found.

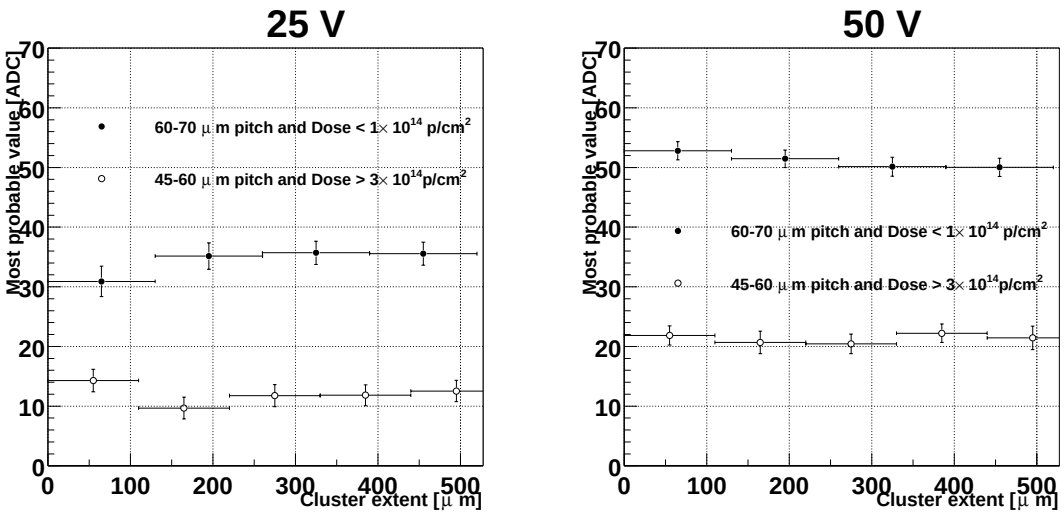

(a)

(b)

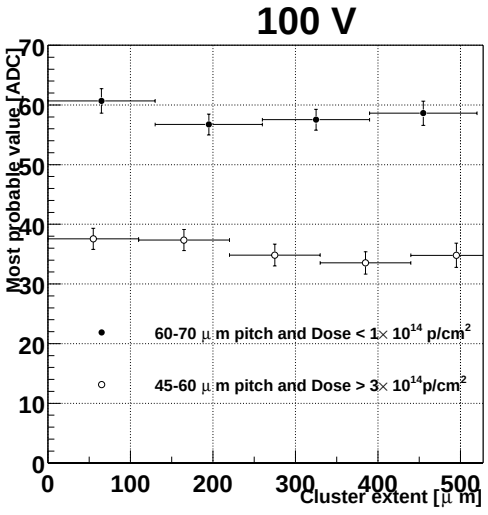

(c)

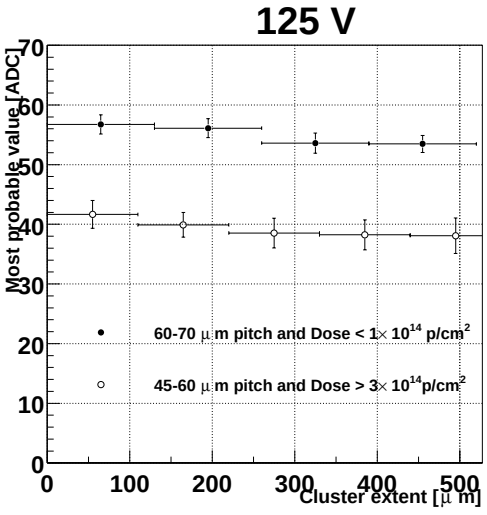

(d)

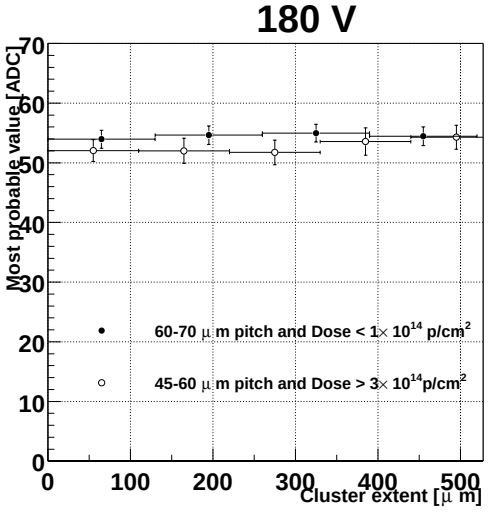

(e)

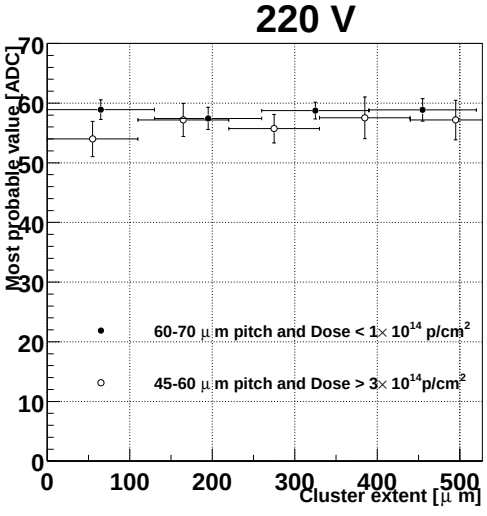

(f)

Figure 15: The cluster extent at different voltages: (a) 25 V, (b) 50 V, (c) 100 V, (d) 125 V, (e) 180 V and (f) 220 V

As mentioned in Section 4 there were two other chips operational in the beam, these are discussed below.

Chip 2 was connected to the innermost region. No tracks traversed this region. However, it is possible to look at the noise from the chip. Displayed in Figure 16 is the noise on chip 2 (channels 128-256) and chip 3 (channels 256-384) for various voltages. As the voltage was increased to 100 V a block of about 25 channels (around channels 155-180) in chip 2 became very noisy. At 180 V all of chip 2 becomes slightly more noisy and, on raising the voltage to 220 V, this effect becomes very significant. The noise level was not significantly changed by the common mode correction at any voltage. Calculating the common mode correction separately for the block of noisy channels and the rest of the chip provides no improvement. The laboratory tests performed on this chip showed a normal noise and gain behaviour.

It is not known if this was a problem specific to this particular test detector or this particular chip, or if it occurs commonly for this design. However, similar phenomena have been observed in ATLAS *n*–on–*n* prototype detectors [16] and attributed to certain strips exhibiting microdischarge noise [15] after irradiation. This phenomenon is known to be a particular risk for *n*–on–*n* detectors, where the field develops from the segmented side of the detector after type inversion, and high field regions can appear, for instance at the p-stops. There are various design techniques which can protect against this [17], such as the use of p-spray and/or field plates. Another possible explanation, at least for the block of noisy channels, is that the presence of a bad channel ('pin-hole') leads to a large current into the chip, thus affecting the noise level of this and nearby channels.

Chip 0 was connected to the non-irradiated side of the detector, and a similar amount of data with tracks was taken with this chip as for chip 3. It exhibited a different pulse shape to that observed for chip 3 (see Figure 17), and also had increased common mode. The peak value is about 2/3 of that expected and the peak of the signal is shifted to about 10 ns later than in chip 3. The observed pulse shape differs significantly from the smooth function observed in chip 1 and in the non-irradiated timing station. The reason for this problematic behaviour has not yet been understood although laboratory tests are underway.

11 Conclusions

A 300 μm thick *n*–on–*n* Hamamatsu LHCb VELO PR-01 prototype detector has been irradiated non-uniformly up to levels of 4×10^{14} protons/cm^2 and tested with beams of minimum ionising particles, using LHC speed SCT128A electronics.

The signal-to-noise for the detector at full charge collection efficiency was measured to be 21.5. The only potential problem seen with the detector is the development of a noisy region of about 25 strips as the voltage is increased. Hence, it is important to monitor the strip-by-strip noise performance after irradiation of future prototypes for as many detectors as possible.

The depletion voltage for irradiation levels of $3 - 4 \times 10^{14}$ protons/cm^2 was found to be approximately 175 V with full charge collection achieved at 220 V. Section 3.2 reports that measurements from the ROSE collaboration show, that for diodes with a similar level of irradiation, the expected depletion voltages are about 110 V for the best oxygenated samples and about 380 V for standard silicon. Hence the depletion voltage of this detector

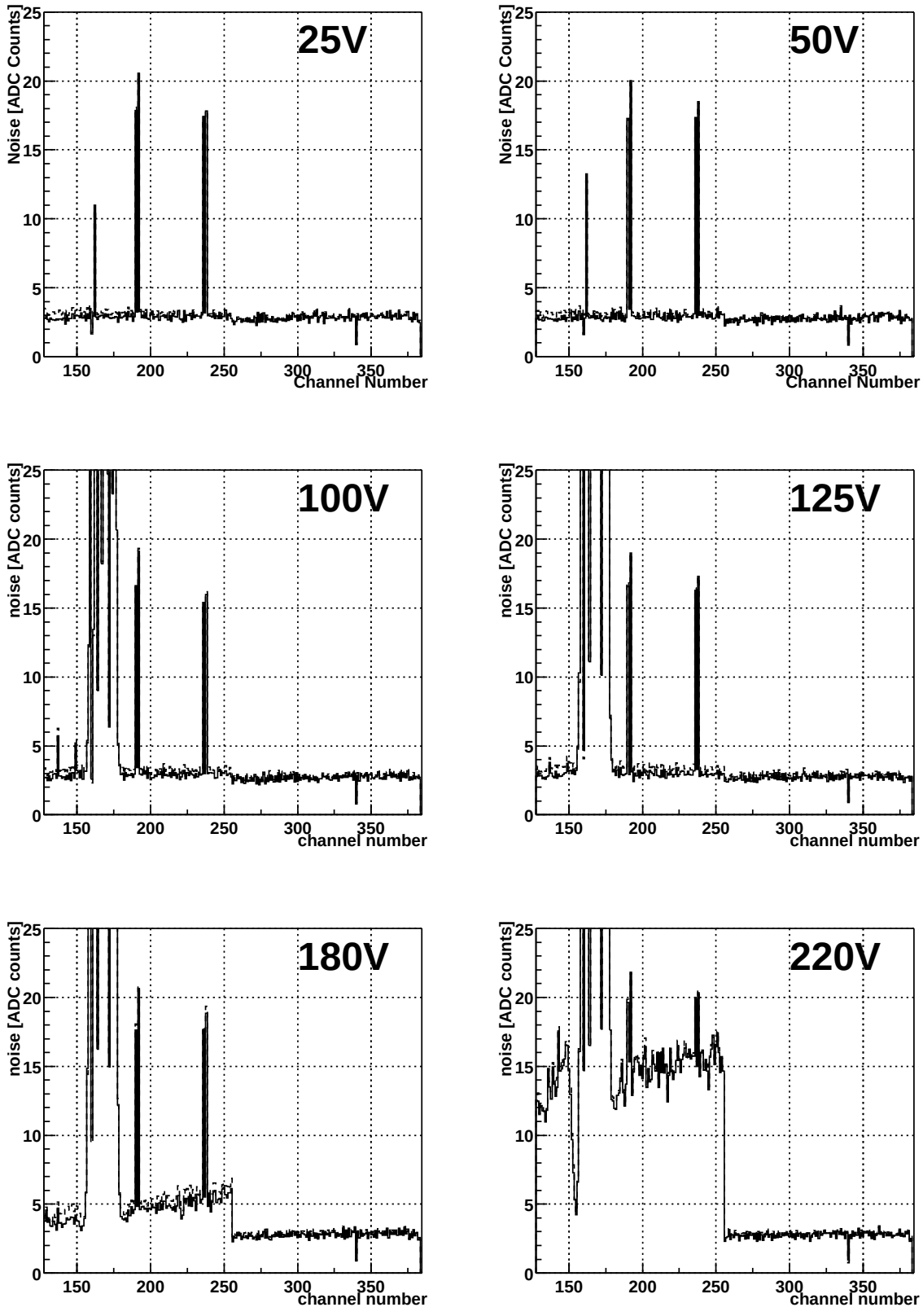

Figure 16: Noise measured in Chip 2 (channels 128-255) and Chip 3 (channels 256-384) before common mode correction (dotted line) and after common mode correction (solid line) for different voltages.

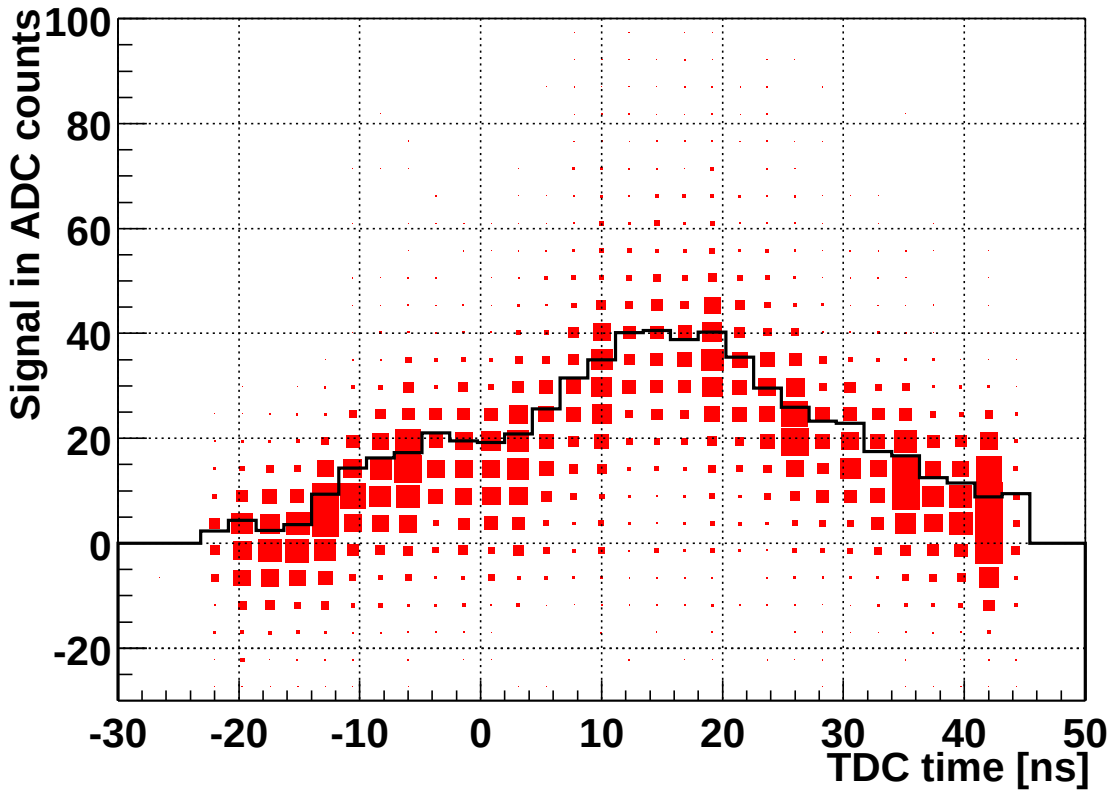

Figure 17: Pulse shape seen for chip 0, with the result of a Landau fit in each bin superimposed.

compares very favourably in spite of the fact that it is not oxygenated. The irradiation level corresponds to about 2 years of operation in LHCb.

The focussing of the observed clusters was measured, and it was found that even if there is charge loss due to underdepletion after irradiation, the clusters remain fully focussed. Hence, there should be no loss in resolution even at the finest pitches: our previous results demonstrate this can be expected for an n–on–n detector [14]. The narrow cluster width also contributes to the good efficiency performance observed for this detector. For a signal-to-noise cut of 3 the detector is fully efficient under 50 V depletion even in the most highly irradiated region. Indeed the possibility to operate the n–on–n detector under-depleted in the most heavily irradiated regions may allow the possibility to tune the bias voltage of the sensors to avoid micro-discharge noise and still obtain a good performance.

The results show that the n–on–n design will survive for at least 2 years in LHCb conditions with negligible deterioration. Due to the safety factor given by the fact that the sensor appears fully efficient even when at $\sim 40\%$ underdepletion, 3-4 years operation could be envisaged.

12 Acknowledgements

We would like to thank Lau Gatignon, Rolf Lindner and the staff of the CERN-PS accelerator for their support during the test-beam. We also very much appreciate the work of Angelo Gandi, Rui de Oliveira and Antonio Teixeira in the CERN Photomechanical workshops (EST-SM-CI), and Alan Honma and Enrico Chesi, also at CERN, for wire bonding and hybrid design. We are very grateful to Jean-Rene Moser and in the Lausanne workshop. Thanks to Michael Moll for his assistance with the annealing studies.

References

[1] Further details are available at the URL http://www.ph.liv.ac.uk/lhcb/

[2] *Study of Vertex silicon Detectors For LHC Experiments* , S. Saladino, PhD Thesis, Università Degli Studi Di Bari, 1999

[3] *Detector Geometry - Vertex Locator test-beam software description* , C. Parkes, LHCb-2000-096

[4] *Measurement of the Irradiation Profile at the PS Beam* , G. Casse *et. al.*, LHCb-2001-020

[5] *SCTA - A rad-hard BiCMOS analogue readout ASIC for the ATLAS semiconductor tracker* , F. Anghinolfi *et. al.*, IEEE Transactions on Nuclear Sciences, Vol. 44, 1997

[6] *Radiation Damage in Silicon Particle Detectors* , M. Moll, DESY-THESIS-1999-040 *Radiation Hardness of Silicon Detectors - a challenge from high-energy physics* , G. Lindstroem, M. Moll, E. Fretwurst, NIM A 426 (1999) 1

[7] 3^{RD} *RD48 Status Report* , F. Lemeilleur *et. al.* CERN/LHCC 2000-009

[8] *ATLAS irradiation studies of n–in–n and p–in–n silicon microstrip detectors* , P. Allport *et. al.*, NIM A 435 (1999) 74

[9] *Study of resolution of VELO test-beam telescope* , V. Wright *et. al.*, LHCb-2000-103

[10] *VELO telescope resolution and efficiency measurements* , P. Bartalini *et. al.*, LHCb-2000-099

[11] *Track Fit - Vertex Locator test-beam software description* , C. Parkes, LHCb-2001-038

[12] *The Performance of the SCT128A ASIC when reading out irradiated and non-irradiated VELO prototype detectors* , M. Charles *et. al.*, LHCb-2001-041

[13] *Performance of an irradiated p–on–n Micron prototype VELO detector* , T.Bowcock *et. al.*, LHCb-2001-040

[14] Charge collection efficiency and resolution of an irradiated double sided silicon microstrip detector operated at cryogenic temperatures , P. Bartalini *et. al.*, NIMA 440 (2000) 17-37

[15] *Micro-discharge noise and radiation damage of silicon microstrip sensors* , T. Ohsugi *et. al.*, NIM A 383 (1996) 166-173

[16] *A comparison of the performance of irradiated p-in-n and n-in-n silicon microstrip detectors read out with fast binary electronics* , P.P. Allport *et. al.*, NIM A 450 (2000) 297-306

[17] *Design optimization of radiation-hard, double-sided, double-metal, AC-coupled silicon sensors* , T. Ohsugi *et. al.*, NIM A 436 (1999) 272-280